Research Square

Preprints are preliminary reports that have not undergone peer review.
They should not be considered conclusive, used to inform clinical practice,
or referenced by the media as validated information.

Exploring the Molecular and Biochemical Mechanisms of Aromasin in Modulating COX-2/iNOS for Alzheimer's Disease-Associated Synaptic Dysfunction: An In Silico Drug Repurposing Study

Devesh Singh Baral
Laxman Singh Mahar Campus, Pithoragarh
Rakesh Verma
rv.pith@gmail.com

Laxman Singh Mahar Campus, Pithoragarh

Research Article

Keywords: Drug Repurposing, ADMET Profiling, Virtual Screening

Posted Date: August 18th, 2026

DOI: https://doi.org/10.21203/rs.3.rs-10701602/v1

License: This work is licensed under a Creative Commons Attribution 4.0 International License.
Read Full License

Additional Declarations: No competing interests reported.

Exploring the Molecular and Biochemical Mechanisms of Aromasin in Modulating COX-2/iNOS for Alzheimer's Disease-Associated Synaptic Dysfunction: An In Silico Drug Repurposing Study

Devesh Singh Baral, & Rakesh Verma*

Department of Zoology, S.S.J. University, L.S.M. Campus, Pithoragarh (262502), Uttarakhand, India.

[Corresponding author *] Email: rv.pith@gmail.com, Contact no +91-9897368158

[ORCiD DSB: 0009-0005-6149-8986, ORCiD RV: 0009-0002-2891-419X]

Exploring the Molecular and Biochemical Mechanisms of Aromasin in Modulating COX-2/iNOS for Alzheimer's Disease-Associated Synaptic Dysfunction: An In Silico Study

Abstract:

Cyclooxygenase-2 (COX-2) and inducible nitric oxide synthase (iNOS) are central regulators of synaptic homeostasis, plasticity, and dysfunction during Alzheimer's disease (AD) progression. Dysregulation of this axis promotes oxidative stress, neuronal injury, impaired synaptic signalling, and cognitive decline. This study aimed to identify a single drug capable of simultaneously modulating the COX-2/iNOS using an in silico drug-repurposing strategy. A library of 3,193 clinically approved compounds was screened, 411 candidates predicted to cross the blood-brain barrier. These compounds were evaluated using molecular docking, ADMET profiling, molecular dynamics simulations, and MM-PBSA free-energy calculations. Aromasin emerged as the most promising candidate, showing strong docking affinities for COX-2 (-9.00 kcal/mol) and iNOS (-7.47 kcal/mol), along with favourable pharmacokinetic properties and predicted CNS safety. MD simulations demonstrated stable protein-ligand complexes, with average RMSD values of ~0.09 nm (COX-2) and ~0.65 nm (iNOS), supported by RMSF, SASA, hydrogen-bonding, and radius of gyration analyses. PCA indicated ligand-induced stabilization, with the first two eigenmodes capturing ~40% of conformational variance. FEL analysis revealed deeper, localized minima upon Aromasin binding, consistent with enhanced thermodynamic stability. MM-PBSA calculations confirmed favourable binding free energies for COX-2 (-24.95 kcal/mol) and iNOS (-21.41 kcal/mol), positioning Aromasin as a promising repurposed modulator for AD-associated synaptic dysfunction. Mechanistically, Aromasin occupied the catalytic pockets through hydrophobic and hydrogen-bond interactions, while dynamic analyses indicated coordinated residue motions and restricted conformational sampling, suggesting that dual target engagement may modulate interconnected inflammatory, oxidative, and nitrosative signalling pathways underlying AD-associated synaptic dysfunction.

Keywords: Drug Repurposing, ADMET Profiling, Virtual Screening

Conflict of Interest:

The authors declare no conflict of interest.

1. Introduction:

Alzheimer's disease (AD) is the leading cause of dementia worldwide (WHO, 2024). Despite extensive research, its multifactorial etiology remains incompletely understood (Samantha et al., 2022). Growing evidence indicates that early synaptic dysfunction and impaired neuronal plasticity are central to AD pathogenesis, often preceding neuronal loss and cognitive decline (Torres et al., 2020). Synapses, as the structural and functional units of learning and memory, are particularly vulnerable, and their disruption closely correlates with the severity of cognitive impairment in AD (Shankar et al., 2009). Altered synaptic signalling, reduced dendritic spine density, and disrupted neurotransmitter homeostasis impair activity-dependent plasticity mechanisms such as long-term potentiation (LTP) and long-term depression (LTD), ultimately weakening neural networks (Lisman, 2017). These deficits are further exacerbated by sustained cellular stress responses such as oxidative stress and endoplasmic reticulum (ER) stress within the central nervous system (CNS), which compromise synaptic maintenance and remodelling (Christoffel et al., 2011). Key molecular mediators, including cyclooxygenase-2 (COX-2) (Moussa & Dayoub, 2023) and inducible nitric oxide synthase (iNOS) (Zhang et al., 2024), have been implicated in dysregulated synaptic transmission and plasticity, thereby contributing to synaptic failure and neurodegeneration in AD.

COX-2 is constitutively expressed in the CNS, particularly in excitatory neurons of the hippocampus and cerebral cortex, where it supports activity-dependent synaptic signalling, long-term plasticity, and cerebral blood flow regulation under physiological conditions (Stefanovic et al., 2006; Yang & Chen, 2008). By Converting arachidonic acid into prostaglandins, COX-2 modulates neurotransmission and synaptic responsiveness, thereby fine-tuning neuronal excitability (Kaufmann et al., 1996). Dysregulated COX-2 activity leads to excessive prostaglandin E_2 (PGE_2) production, which disrupts intracellular calcium homeostasis, increases oxidative stress, and facilitates excitotoxic signalling. These processes are closely associated with tau pathology, amyloid-β accumulation, and progressive synaptic loss in AD (Woodling et al., 2016). The functional duality of COX-2 is further influenced by NMDA receptor localization synaptic signalling supports physiological plasticity, whereas extra-synaptic activation promotes maladaptive prostaglandin production and neurotoxic outcomes during disease progression (Woodling et al., 2016).

Nitric oxide (NO), synthesized by nitric oxide synthases (NOS), is a critical regulator of neuronal communication, synaptic plasticity, and neurovascular coupling (Iova et al., 2023). Under physiological conditions, basal NO levels facilitate synaptic transmission and act as a diffusible signalling molecule that supports neuronal adaptability. In contrast, excessive NO production, particularly mediated by iNOS, disrupts neuronal signalling homeostasis and contributes to neurotoxicity (Iova et al., 2023). Elevated NO rapidly reacts with superoxide radicals to form peroxynitrite ($ONOO^-$), a highly reactive species that induces oxidative damage to proteins, lipids, and DNA, promotes mitochondrial dysfunction, and activates poly(ADP-ribose) polymerase (PARP), ultimately compromising synaptic integrity and neuronal survival (Pacher et al., 2007). Thus, NO exhibits a concentration-dependent dual role, it functions as a neuromodulator at physiological levels but acts as a potent mediator of synaptic toxicity when overproduced (Tiwari et al., 2021). Although transient iNOS expression may contribute to neuroprotection or developmental processes, its sustained activation in the mature brain is predominantly associated with pathological neuroinflammatory conditions and progressive neurodegeneration (Chachlaki et al., 2020). Given the high cost and time associated with de novo drug development, drug repurposing

presents a viable strategy to identify existing compounds with known safety profiles that may interact with these targets.

Despite the established roles of COX-2 and iNOS in neuroinflammation, oxidative stress, and synaptic dysfunction in Alzheimer's disease (AD), their simultaneous targeting through drug repurposing remains insufficiently explored. Given the interconnected nature of inflammatory and oxidative pathways in AD, we hypothesized that approved drugs capable of modulating both targets could provide potential multi-target therapeutic candidates. Accordingly, we screened approved drugs against COX-2 and iNOS to identify potential dual-target candidates, followed by molecular docking, molecular dynamics simulations, MM/PBSA binding free-energy analysis, and ADMET profiling to characterize their binding behaviour, dynamic stability, energetic favourability, and pharmacokinetic properties. This integrated approach aims to provide molecular-level insights into potential dual-target modulation of COX-2/iNOS and establish a computational basis for further experimental evaluation in AD.

2. Materials and Methods:

2.1 Collection of Clinically Approved Drugs:

SelleckChem (https://www.selleckchem.com/) provided a chemical library of authorized medications. Structures of approved drugs, along with molecular weight (MW), molecular formula (MF), and SMILES notations, were collected for evaluation. All compounds were downloaded in .sdf format for subsequent docking and MD studies.

2.2 Drug-likeliness:

An initial drug-likeness screening was conducted to exclude compounds lacking CNS-relevant properties, using a modified Lipinski's Rule of Five tailored for central nervous system (CNS) activity. Selection criteria included molecular weight (MW) < 450 Da, hydrogen bond acceptors (HBA) < 7, hydrogen bond donors (HBD) < 3, fewer than 8 rotatable bonds, Log P ≤ 4, topological polar surface area (TPSA) < 90 Å², and predicted blood-brain barrier (BBB) permeability (Pajouhesh et al., 2005). All parameters were evaluated using the SwissADME web tool (https://www.swissadme.ch/).

2.3 Receptor and Ligand Preparation for Docking:

All approved drugs selected for docking were energy-minimized using the Universal Force Field (UFF) for 250 steps, then converted to .pdbqt format with Open Babel (O'Boyle et al., 2011). Protein structures of COX-2 (PDB ID: 5IKQ, 2.41 Å) and iNOS (PDB ID: 3E7G, 2.20 Å) were obtained from the RCSB Protein Data Bank (https://www.rcsb.org) and further energy-minimized in UCSF Chimera (https://www.cgl.ucsf.edu/chimera/) using the steepest descent algorithm (500 steps, step size 0.02 Å) (Baral & Verma, 2025a; Pakrashy et al., 2022). Before docking, heteroatoms and water molecules were removed, and the protein structures were protonated (Baral & Verma, 2025b; Rana et al., 2025). Co-crystallized ligands JMS (meclofenamic acid) for COX-2 and AR-C95791 for iNOS were extracted from their respective complexes and used as reference inhibitors for comparative analyses.

2.4 Active Site Determination and Molecular Docking:

The binding pockets of COX-2, and iNOS were defined based on the spatial orientation of their respective co-crystallized ligands and used for grid generation. Docking grids were centred at COX-2 (x = 21.598, y = 51.877, z = 17.696; 20 Å), and iNOS (x = 55.396, y = 21.119, z = 78.997; 20 Å). Molecular docking was performed using AutoDock Vina v1.1.2 (Eberhardt et al., 2021) with an exhaustiveness of 16 and an energy range of 4 kcal/mol, while maintaining uniform grid parameters for methodological consistency. Post-docking interaction profiling and 2D/3D visualizations were conducted using BIOVIA Discovery Studio (2025) (https://www.3ds.com/).

2.5 Redocking:

Redocking was performed for each of the target proteins using AutoDock Vina (Eberhardt et al., 2021) to validate the docking procedure. UCSF Chimera (https://www.cgl.ucsf.edu/) was used to calculate the root-mean-square deviation (RMSD) between the redocked poses and their corresponding crystallographic conformations, thereby assessing the reliability of the docking protocol. An RMSD value of < 2.0 Å between the redocked pose and the crystallographic conformation was considered acceptable validation.

2.6 ADMET:

Key pharmacokinetic and drug-likeness parameters were evaluated using SwissADME (http://www.swissadme.ch/), including assessment of P-glycoprotein (P-gp) substrate/inhibitor status, gastrointestinal (GI) absorption, bioavailability score, cytochrome P450 enzyme (CYP2C19, CYP3A4, CYP2D6, CYP1A2, CYP2C9) inhibition, and PAINS alerts (Daina et al., 2017). Toxicity profiles, including hepatotoxicity, carcinogenicity, immunotoxicity, and mutagenicity, were assessed using ProTox 3.0 (https://tox.charite.de/protox3/) (Banerjee et al., 2024). Compounds were retained if they violated no more than two of the following parameters: P-gp substrate status, CYP inhibition, low bioavailability score, or PAINS alerts. Compounds with more than two violations were excluded.

2.7 MD:

Molecular dynamics (MD) simulations were conducted using GROMACS 2024.5 (https://www.gromacs.org/). Each system was solvated in a cubic box, neutralized with counter-ions, and prepared with the CHARMM36 force field (Huang et al., 2013) and the TIP3P water model (Khalid et al., 2022). Ligand topologies were generated using SwissPARAM (http://swissparam.ch/). Energy minimization was performed for 50,000 steps using the steepest descent algorithm (Rana et al., 2025). NVT equilibration was carried out at 300 K for 50,000 steps using the V-rescale thermostat, followed by NPT equilibration at 1 bar with the Parrinello-Rahman barostat (Bussi et al., 2007, Parrinello & Rahman, 1981). A 100 ns production run was executed under NPT conditions with a 2 fs time step. Post-simulation analyses included quantification of hydrogen bonds (H-bonds), root mean square deviation (RMSD), root mean square fluctuation (RMSF), radius of gyration (Rg), and solvent-accessible surface area (SASA), all calculated using GROMACS built-in gmx tools. Advanced trajectory analyses were conducted using the Bio3D package in R (v4.5.1) (Shjaerven et al., 2014), including principal component analysis (PCA), dynamic cross-correlation matrix (DCCM) analysis, and free energy landscape (FEL) construction to characterize collective motions, residue-residue dynamics, and conformational energy minima (Baral & Verma, 2025a; Islam et al., 2025).

2.8 Free Energy Estimation:

GMX-MMPBSA (https://valdes-tresanco-ms.github.io/) was used to calculate binding free energy, a GROMACS-compatible end-state free-energy calculation tool that efficiently computes MM/PBSA-based energetics (Valdes-Tresanco et al., 2021). A total of 301 uniformly spaced frames were chosen from the last 30 ns of each simulation for analysis.

3. Results:

3.1 Clinically Approved Drugs:

A dataset of 3,193 approved drugs, selected from the larger SelleckChem collection of over 20,000 FDA-approved therapeutic agents, was obtained. This dataset represents a clearly defined subset. The clinical safety and regulatory compliance of these compounds have been validated by major authorities, including the U.S. Food and Drug Administration (FDA), the European Medicines Agency (EMA), the Heads of Medicines Agencies (HMA), the Chinese Food and Drug Administration (CFDA), and the Pharmaceuticals and Medical Devices Agency (PMDA) of Japan. This subset of compounds formed the basis for subsequent computational screening (Supplementary Table S1).

3.2 Drug likeliness:

All 3,193 compounds were screened for CNS drug potential using a modified Lipinski-based filter. The molecular weights ranged from 42.39 to 4177.76 Da, with 2,200 compounds falling below the optimal 450 Da threshold. TPSA values spanned 0-400.5 Å², and 1,856 compounds were within the ≤90 Å² limit. Log P values ranged from -5.92 to 12.16, with 1,901 compounds in the optimal 0-4 range. Hydrogen bond acceptors and donors reached maxima of 24 and 17, respectively, and 2,234 and 2,324 compounds met the criteria. Rotatable bonds extended up to 35, with 2,401 compounds satisfying preferred CNS thresholds. Overall, 822 compounds were predicted to cross the blood-brain barrier, and upon integrating all parameters 411 were identified as potential CNS-active candidates (Supplementary Table S1). These candidates were further prioritized based on drug-likeness, docking performance, and ADMET profiles (Table 1).

3.3 Molecular Docking:

A library of 411 CNS drug-like compounds was docked against COX-2, and iNOS (Supplementary Tables S2-S3). Based on docking performance, the top 20 ligands per receptor were shortlisted for ADMET evaluation, followed by 2D and 3D binding-pose analyses of the filtered hits.

For COX-2, post-ADMET screened compounds exhibited docking scores ranging from -9.40 to -8.80 kcal/mol (Table 2), indicating strong binding affinity within the active site. Compound 268 interacted with 19 residues, followed by compound 505 with 18 and compound 41 with 17 interacting residues, reflecting stable ligand accommodation. Notably, compound 41 additionally formed a carbon-hydrogen bond at a distance of 2.69 Å, suggesting a favourable contribution to binding stabilization. Compound 1366, although showing slightly lower affinity, still maintained interactions with 15 residues primarily through van der Waals and hydrophobic contacts. Importantly, key residues such as Ser353, Leu384, Trp387, Met522, and Ser530 were consistently conserved across all ligand complexes, highlighting their critical role in maintaining structural stability and facilitating ligand binding within the COX-2 active site (Figure 1).

Similarly, in the case of iNOS (Figure 2), docking energies ranged from -8.35 to -7.13 kcal/mol, suggesting moderate to strong binding interactions. Compound 41 demonstrated interaction with 13 residues through a combination of hydrogen bonding and van der Waals forces, including a short contact of 2.21 Å, indicative of tight active-site fitting and enhanced interaction strength. Other leading compounds, including 981, 2037, and 98, interacted with approximately 13-15 residues, engaging both polar and hydrophobic amino acids to stabilize the complexes. Furthermore, conserved residues such as Trp346, Tyr347, Gln263, Pro350, Val352, Glu377, Arg388, and Asp382 were consistently involved across multiple ligand interactions, reinforcing their essential role in ligand recognition, binding specificity, and catalytic site architecture.

3.4 Redocking:

The co-crystallized ligands were redocked into their respective native binding sites to validate the docking protocol. For COX-2, the native ligand JMS (meclofenamic acid) exhibited a docking score of -9.10 kcal/mol, along with excellent pose overlap (RMSD 0.11 Å) (Figure 3). The docked and native complexes shared all 18 interacting residues through hydrogen bonds, alkyl, and π-alkyl interactions, confirming the reliability of the docking protocol. Redocking of AR-C95791 into iNOS resulted in a docking score of -6.18 kcal/mol and an RMSD of 0.65 Å (Figure 4), with 15 shared interacting residues, thereby validating the accuracy of the predicted binding pose.

3.5 Pharmacological property:

A comprehensive ADME/T analysis was conducted for the top 20 scoring compounds per receptor (based on doc), with detailed data in (Supplementary Tables S4-S5) and a summary in Table 3. Absorption was evaluated based on GI absorption and P-gp substrate status. All selected compounds exhibited high GI absorption, while three of nine were identified as P-gp substrates, indicating possible efflux liability. Metabolic assessment against major cytochrome P450 isoenzymes (CYP1A2, CYP2C19, CYP2C9, CYP2D6, and CYP3A4) revealed minimal inhibitory interactions, suggesting a low risk of cytochrome-mediated drug-drug interactions. Toxicity profiling across hepatotoxicity, carcinogenicity, mutagenicity, and cytotoxicity endpoints showed no predicted adverse effects. All candidates demonstrated good oral bioavailability (≥0.55), and none triggered PAINS alerts, supporting genuine biological activity. Reference drugs for COX-2, and iNOS were evaluated using the same criteria. Although the screened compounds showed favourable GI absorption suitable for oral use. The reference COX-2 inhibitor showed a high risk of drug–drug interactions and was predicted to cause hepatotoxicity, whereas the iNOS references displayed acceptable metabolic profiles. (Table 3).

3.6 Stability Analysis:

To assess the protein's overall stability, a 100 ns MD trajectory was examined. Important metrics like RMSD, RMSF, H-bonds, Rg, and SASA were calculated to assess protein stability. These analyses were performed for the protein in three states; the apo form, the ligand-bound form (compound 41), and the control form (with the co-crystallized ligand present). Representative structures of each ligand-target complex obtained during the MD simulation at 0, 50, and 100 ns are provided in Supplementary Table S6.

3.6.1 RMSD Analysis:

For COX-2 (Figure 5A), the apo system maintained an average RMSD of ~0.20 nm throughout the simulation, indicating inherent structural stability. In comparison, the compound-41 complex exhibited the lowest deviation (~0.09 nm), suggesting enhanced stability upon ligand binding and minimal conformational fluctuation. The meclofenamic acid complex, however, showed a slightly higher deviation (~0.28 nm), reflecting comparatively greater structural flexibility. Overall, this establishes the stability trend as; compound-41 > apo > reference ligand, highlighting the favourable stabilizing effect of compound-41 within the COX-2 binding pocket. In the case of iNOS (Figure 5B), the apo protein remained relatively stable with an average RMSD of ~0.21 nm. In contrast, both the compound-41 and AR-C95791 complexes exhibited higher deviations (~0.65 and ~0.71 nm, respectively), indicating increased structural rearrangements upon ligand binding. This behaviour is consistent with ligand accommodation within a comparatively larger and more flexible active site, allowing greater conformational adaptability during the simulation period.

3.6.2 RMSF Analysis:

For COX-2 (Figure 6A), the apo and compound-41 complexes exhibited comparable RMSF profiles, with maximum fluctuations of ~0.28 nm. Peaks at residues ~20-50, ~130-140, ~180-190, ~240-250, and ~330-350 indicate regions involved in ligand accommodation or conformational flexibility. In contrast, the meclofenamic acid-bound system showed greater flexibility, with RMSF values reaching ~0.50 nm at regions ~1-50, ~90-110, ~130-140, ~240-250, ~325-340, and ~510-520, suggesting stronger ligand-induced motions. For iNOS (Figure 6B), RMSF patterns were similar across systems, with the apo protein displaying the highest flexibility at the C-terminus (~1.02 nm), while most residues fluctuated below ~0.50 nm. Despite overall structural stability, regions ~25-40, ~170-190, and ~320-340 remained relatively dynamic, likely reflecting conformational adjustment.

3.6.3 H-bond Analysis:

In COX-2 (Figure 7A), compound 41 formed up to three hydrogen bonds, most frequently between 20-40 ns, with brief occurrences at ~50-55 ns and ~85 ns; two bonds remained stable throughout the simulation. Meclofenamic acid formed up to four hydrogen bonds, mainly during the initial 0-20 ns, with two persisting for most of the trajectory, indicating sustained interactions for both ligands. For iNOS (Figure 7B), both ligands formed a maximum of three hydrogen bonds. The reference ligand reached this only once (~50 ns), whereas compound 41 briefly formed three at ~1 ns and again near 70 ns; however, two hydrogen bonds dominated for most of the simulation, reflecting stable active-site engagement.

3.6.4 Rg Analysis:

For COX-2 (Figure 8A), the apo protein exhibited an average Rg of 2.45 nm, while both the compound-41 and meclofenamic acid complexes showed comparable values of 2.46 nm, indicating negligible changes in structural compactness upon ligand binding. This minimal variation suggests that ligand association does not significantly disturb the overall folding of the protein. Furthermore, the consistent Rg profile throughout the simulation reflects the maintenance of structural integrity in all systems. The absence of major fluctuations also indicates that both ligands are well accommodated without inducing global conformational changes. Similarly, the apo iNOS system displayed an average Rg of 2.30 nm, whereas the compound-41 and AR-C95791 complexes maintained values of 2.31 nm (Figure 8B). This further supports the notion that ligand binding preserves the compactness and structural stability of the iNOS protein during the simulation.

3.6.5 SASA Analysis:

For COX-2 (Figure 9A), the apo protein showed an average SASA of 249.67 nm², while the compound-41 and meclofenamic acid complexes averaged 253.86 nm² and 255.72 nm², respectively, indicating only minor ligand-induced fluctuations. These slight increases in SASA suggest limited exposure of surface residues upon ligand binding. However, the overall consistency in SASA values indicates that no major unfolding or structural disruption occurred. The observed variations may be attributed to minor rearrangements in surface-accessible regions during the simulation. A similar trend was observed for iNOS (Figure 9B), with average SASA values of 213.25 nm² (apo), 215.20 nm² (compound 41), and 217.19 nm² (AR-C95791). This consistency further confirms that ligand binding does not significantly alter the solvent accessibility or overall structural stability of the protein systems.

3.6.6 PCA:

PCA was used to assess ligand-induced changes in the collective motions of COX-2, and iNOS by projecting MD trajectories onto the first two principal components (PC1 and PC2), which capture dominant conformational variance (Figure 10). In COX-2, the apo system showed broad sampling, with PC1 (30.46%) and PC2 (9.27%) accounting for ~39.7% of total variance, reflecting high intrinsic flexibility. Binding of compound 41 redistributed variance across PC1 (28.99%) and PC2 (11.36%), indicating more ordered essential dynamics, whereas the reference-bound system was dominated by PC1 (47.24%) with reduced PC2 motion (9.59%), consistent with constrained single-mode behaviour. The apo iNOS system also displayed extensive flexibility (PC1: 36.04%, PC2: 10.71%). Compound 41 binding redistributed motion across PC1 (24.67%) and PC2 (15.86%), suggesting stabilization of multiple collective modes, while the reference-bound system showed more restricted dynamics (PC1: 25.40%, PC2: 9.03%).

3.6.7 DCCM:

Residue-wise correlated and anti-correlated motions in COX-2, and iNOS were examined using DCCM (Figure 11), where positive (red) and negative (blue) values represent concerted and opposing motions, respectively. Although most correlations were local, apo COX-2 exhibited pronounced long-range anti-correlations between residues ~100-150 and between the N-terminal (~1-50) and C-terminal (~450-520) regions, indicating high inter-domain flexibility. Binding of compound 41 markedly reduced these anti-correlations, particularly within residues ~100-150, while enhancing positive correlations across ~100-300, suggesting improved intra-domain communication. In contrast, the reference-bound COX-2 system partially restored anti-correlations, with persistent opposing motions between the mid-domain (~70-200) and C-terminal regions. The apo iNOS system showed minimal anti-correlated motions, reflecting limited inter-domain adaptability, whereas compound 41 binding strengthened positive correlations across residues ~150-260 and further reduced anti-correlations, consistent with stabilized cooperative dynamics. The reference-bound iNOS system displayed an intermediate pattern with retained correlated regions.

3.6.8 FEL:

FEL maps of COX-2, and iNOS were projected onto the first two principal components (PC1 and PC2) to evaluate conformational stability and transitions during MD simulations (Figure 12). Low-energy (blue) regions represent

thermodynamically favourable states, whereas high-energy (red) regions indicate less favoured conformations. The apo COX-2 system displayed a rugged landscape with multiple broad minima across the PC1-PC2 plane, reflecting high conformational variability and frequent transitions between metastable states. In contrast, compound 41 binding markedly reshaped the landscape, producing fewer and deeper minima indicative of stabilized conformations and reduced conformational entropy, while the reference-bound system showed an intermediate profile with smaller energy basins. The apo iNOS system exhibited dispersed low-energy basins separated by high-energy barriers, consistent with pronounced flexibility. Compound 41 binding generated distinct and deeper minima, indicating confinement of protein dynamics within energetically favourable regions, whereas the reference-bound system remained broader and less well-defined than the compound 41 complex.

3.7 Binding Free Energy:

For COX-2 (Table 4), compound 41 exhibited a total binding free energy of -24.95 kcal/mol, slightly stronger than meclofenamic acid (-23.90 kcal/mol), primarily due to more favourable van der Waals contributions (-40.15 vs -35.47 kcal/mol), indicating tighter hydrophobic packing within the active site. In iNOS, compound 41 showed a markedly stronger ΔG_bind (-21.41 kcal/mol) than AR-C95791 (-13.68 kcal/mol), with van der Waals and polar solvent terms dominating the interaction profile, consistent with a stabilized non-polar interface despite moderate solvation penalties (Figure 13). Overall, MM-PBSA results confirm stable and energetically favourable interactions of compound 41 across all targets, with binding strengths comparable to or exceeding reference inhibitors, particularly for COX-2 and iNOS (Table 4). The predominance of van der Waals contributions supports the formation of stable, well-packed ligand-protein interfaces.

4. Discussion: (mechanism based)

Synaptic homeostasis, plasticity, and dysfunction are regulated by tightly interconnected receptor-mediated and intracellular signalling networks that coordinate neuronal activity, metabolic balance, and adaptive plasticity. Among these networks COX-2, and iNOS, play central roles as activity-dependent regulators of oxidative stress, neuroinflammatory signalling, and neuronal injury (Moussa & Dayoub, 2023; Zhang et al., 2024). Dysregulation of these pathways disrupts calcium homeostasis, compromises mitochondrial integrity, and amplifies oxidative and nitrosative stress, collectively driving synaptic instability, impaired plasticity, and progressive neurodegeneration (Woodling et al., 2016). Importantly, these mediators do not act in isolation; instead, they converge on shared downstream mechanisms governing receptor trafficking, energy metabolism, and synaptic remodelling. As a result, therapeutic strategies targeting a single pathway often fail to adequately modulate the complex molecular landscape underlying synaptic dysfunction. Consequently, coordinated multi-target modulation has emerged as a more effective approach for restoring synaptic balance than conventional single-target inhibition (Zhang et al., 2023).

In this context, the present study employed a multitarget drug-repurposing strategy, systematically screening approximately 3,193 clinically approved compounds with well-established safety and pharmacokinetic profiles. This approach offers a substantial advantage over de novo drug discovery by reducing developmental cost, risk, and timelines (Kulkarni et al., 2023). Of these compounds, 3,193 were evaluated for CNS drug-likeness using a BBB-optimized Lipinski filter (Pajouhesh et al., 2005), yielding 411 candidates with favourable physicochemical properties, permeability, and CNS relevance. These candidates were subjected to molecular

docking against COX-2, and iNOS, followed by stringent ADMET filtering of the top-ranked ligands. Among all screened molecules, compound 41 emerged as the most robust repurposing candidate, demonstrating strong binding affinity across all targets, high gastrointestinal absorption, acceptable bioavailability, and no predicted mutagenicity, cardiotoxicity, hepatotoxicity, carcinogenicity, or PAINS alerts (Odhiambo et al., 2025). Compound 41 shows favourable predicted ADMET properties and a pharmacokinetic advantage over the COX-2 reference (higher hepatotoxicity risk), while the iNOS reference is acceptable.

Compound 41 achieved docking scores of -9.00, and -7.74 kcal/mol against COX-2, and iNOS respectively, indicating stable and energetically favourable interactions that were comparable to those of established reference inhibitors (Alsedfy et al., 2024). Redocking validation yielded RMSD values below 2.0 Å, confirming accurate pose reproduction and binding-site reliability (de Oliveira et al., 2022). Compound 41 binds COX-2 differently than the reference inhibitor it occupies the central catalytic cavity via hydrophobic contacts (Leu352, Leu384, Trp387, Phe518, Met522, Val523) and a hydrogen bond with Gly526, but lacks the reference inhibitor's key interactions with Tyr385 and Ser530. Despite this, its central pocket occupation and shared residue contacts suggest a valid alternative binding mode. Similarly Compound 41 binds iNOS differently than the standard ligand: it forms a hydrogen bond with Tyr373 and hydrophobic contacts (Val352, Pro350, Phe369), but lacks the standard's key interactions with Tyr347 and Glu377. Despite this, its shared pocket occupation and residue overlaps suggest a credible alternative binding mode for iNOS modulation.

To assess the dynamic stability of the docked complexes, 100 ns molecular dynamics simulations were performed for apo, compound 41-bound, and reference-ligand-bound systems under explicit solvent conditions. RMSD analysis showed that compound 41/COX-2 had the lowest average deviation (~0.09 nm) compared with apo COX-2 (~0.20 nm) and meclofenamic acid (~0.28 nm), indicating greater conformational stability, while compound 41/iNOS showed slightly lower RMSD (~0.65 nm) than AR-C95791 (~0.71 nm), suggesting comparable stability (Ghahremanian et al., 2022). RMSF profiles indicated restrained local flexibility, with compound 41/COX-2 (~0.28 nm) showing lower fluctuations than meclofenamic acid (~0.50 nm), while compound 41 and AR-C95791 produced broadly similar profiles for iNOS (Hassan et al., 2024). Compound 41 also maintained approximately two persistent hydrogen-bond interactions with both targets, supporting sustained ligand engagement during simulation (Li et al., 2022). Rg values remained comparable to the corresponding apo proteins for both COX-2 and iNOS, indicating preservation of global compactness and protein folding (Pandey et al., 2018). Similarly, SASA values showed only minor changes between compound 41-bound and apo systems, suggesting no substantial increase in solvent exposure or structural rearrangement (Ghahremanian et al., 2022). Overall, the MD results support stable compound 41 COX-2 and compound 41 iNOS complexes while preserving the structural integrity and native flexibility of both targets.

Essential dynamics analyses further supported the dynamic stabilization of compound 41-bound complexes. PCA showed a more balanced distribution of collective motions for compound 41 across PC1/PC2 compared with the reference complexes, with COX-2 values of 28.99%/11.36% versus 47.24%/9.59% for the reference and iNOS values of 24.67%/15.86% versus 25.40%/9.03%, suggesting stabilization of multiple collective modes rather than dominance of a single motion (Baral & Verma, 2025a; Islam et al., 2025). Dynamic cross-correlation analysis further indicated reduced long-range anti-correlated motions and enhanced positive correlations across residues ~100–300 in COX-2 and ~150–260 in iNOS, suggesting more coordinated intra-

domain dynamics and residue communication upon compound 41 binding (Dash et al., 2019). Consistently, free energy landscape analysis revealed fewer and deeper low-energy minima for compound 41-bound systems, whereas the reference complexes showed broader and less-defined energy landscapes, indicating restricted conformational sampling and preferential occupancy of energetically favourable states (Islam et al., 2025). Overall, these essential dynamics results support improved conformational coordination and stability of compound 41-bound COX-2 and iNOS complexes. MM-PBSA analysis further supported the favourable binding of compound 41 to both targets, with more favourable binding free energies than the reference inhibitors for COX-2 (-24.95 vs. -23.90 kcal/mol) and iNOS (-21.41 vs. -13.68 kcal/mol), indicating stronger overall energetic stabilization (Genheden & Ryde, 2015). Energy decomposition showed that van der Waals interactions were major contributors, particularly for COX-2, where compound 41 exhibited a more favourable contribution (-40.15 vs. -35.47 kcal/mol), suggesting enhanced hydrophobic packing within the binding pocket (Wang et al., 2022). The substantially greater binding advantage observed for iNOS further indicates that compound 41 may establish energetically favourable ligand–protein interactions across both targets, supporting its potential as a dual-target inhibitor.

Compound 41 was identified as Aromasin, an FDA-approved steroidal aromatase inhibitor widely used in breast cancer therapy (Kittanesh & Gluck et al., 2011). Aromasin displayed favourable ADME properties, high oral bioavailability, and CNS suitability. Although not previously studied as a direct COX-2, and iNOS pathway modulator, its reported effects on oxidative balance, cellular stress responses, and cytokine-associated signalling align well with the present computational findings (Liu & Talalay, 2013). With low discontinuation rates (<5%) and good overall tolerability (Bell et al., 2020), Aromasin represents a practical and accelerated candidate for CNS-directed therapeutic repurposing in synaptic dysfunction related to AD. Exemestane presents a complex pharmacological profile in the context of neurodegeneration. While the present computational analysis predicts its potential to inhibit key inflammatory mediators such as COX-2 and iNOS, which are implicated in synaptic dysfunction and cognitive decline, its established role as an aromatase inhibitor introduces a conflicting biological dimension. Aromatase inhibition leads to reduced oestrogen synthesis, and oestrogens is widely recognized for its neuroprotective effects (Simpkins et al., 2012). This creates a mechanistic paradox in which the predicted anti-inflammatory benefits may be counterbalanced by endocrine-mediated risks. Therefore, the potential neuroprotective role of Exemestane cannot be directly inferred and remains highly context-dependent, warranting further experimental validation.

Overall, the present study fulfilled its aim of investigating the potential of Aromasin (exemestane) against COX-2 and iNOS through an integrated drug-repurposing and computational framework. The combined docking, molecular dynamics, essential dynamics, and MM-PBSA analyses provided a computer-based mechanistic perspective on its target recognition, dynamic stability, residue-level interactions, and binding energetics. The consistent findings across these approaches support the hypothesis that Aromasin may simultaneously modulate COX-2 and iNOS-associated pathways relevant to synaptic dysfunction in AD. While these computational predictions require experimental validation, the favourable binding behaviour and drug-like properties of Aromasin provide a rational basis for further in vitro and in vivo investigation. Thus, this study not only identifies Aromasin as a potential multitarget candidate but also provides a mechanistic computational framework

explaining how its interaction with these targets may contribute to its proposed therapeutic relevance in AD-associated synaptic dysfunction.

5. Conclusion: (toward molecular mechanism)

The present study demonstrates that drug repurposing, supported by an integrated computational framework, provides a rational approach for re-evaluating existing therapeutics as modulators of pathways involved in synaptic homeostasis, plasticity, and dysfunction. Molecular docking analyses indicated strong ligand–receptor complementarity, while redocking procedures confirmed the reliability of the docking protocol. ADMET profiling further suggested favourable pharmacokinetic properties, safety, and CNS compatibility. MD simulations revealed stable protein–ligand interactions under physiological conditions, supported by consistent binding energetics. Importantly, the integration of PCA, DCCM, and FEL analyses provided a mechanistic perspective on Aromasin-mediated target modulation, demonstrating altered collective motions, strengthened residue–residue communication, reduced long-range anti-correlations, and stabilization of energetically favourable conformations compared with the corresponding apo and reference-bound systems. These dynamic changes suggest that Aromasin may modulate the conformational and communication networks of COX-2 and iNOS, providing a mechanistic basis for its potential effects on interconnected pathways associated with synaptic dysfunction. Collectively, these findings support the potential of Aromasin as a repurposed multi-target modulator and provide a computer-based mechanistic framework for understanding its interaction with COX-2 and iNOS, warranting further experimental validation for its possible role in restoring synaptic homeostasis and mitigating synaptic dysfunction in AD.

Supplementary:

A supplementary file has been uploaded with manuscript (Table S1-S6).

Acknowledgements:

The authors would like to acknowledge L.S.M. Campus, Pithoragarh, for providing necessary facilities and support.

Funding:

This work did not receive any external or internal funding.

Author Contribution:

Devesh Singh Baral - Conceptualization, Methodology, Software, Visualization, Formal analysis, Original Draft Preparation

Rakesh Verma - Supervisor, Methodology, Critical Analysis, Review & Editing

Table 1: Physicochemical and BBB permeability assessment of top-ranked compounds

S.No.	Compound ID	Name	Formula	Molecular Weight (< 450 Da)	TPSA (Å^2) (< 90)	LogP (≤ 4)	HBA (< 7)	HBD (< 3)	RB (< 8)	BBB
1.	41	Aromasin (FCE 24304)	$C_{20}H_{24}O_2$	296.40	34.14	2.63	2	0	0	Yes
2.	98	Tropisetron HCl	$C_{17}H_{21}ClN_2O_2$	320.81	41.90	2.24	4	0	3	Yes
3.	268	Progesterone (NSC 9704)	$C_{21}H_{30}O_2$	314.46	34.14	3.67	2	0	1	Yes
4.	505	Estriol	$C_{18}H_{24}O_3$	288.38	60.69	2.70	3	3	0	Yes
5.	981	Neflamapimod (VX-745)	$C_{19}H_9Cl_2F_2N_3OS$	436.26	47.26	2.70	4	0	3	Yes
6.	1366	Sophoridine	$C_{15}H_{24}N_2O$	248.36	23.55	1.19	3	0	0	Yes
7.	2037	Dolasetron Mesylate	$C_{20}H_{24}N_2O_6S$	438.47	62.40	2.78	5	1	3	Yes
8.	2058	Palonosetron	$C_{19}H_{24}N_2O$	296.40	23.55	2.49	3	0	1	Yes
9.	2167	Ethisterone	$C_{21}H_{28}O_2$	312.44	37.30	3.31	2	1	0	Yes

*TPSA = Topological polar surface area, *HBA = Hydrogen bond acceptor, *HBD = Hydrogen bond donor, *RB = Rotatable bonds, *BBB = Blood brain barri

Table 2: Docking score of ADMET passed compounds with respective receptors, COX-2, and iNOS

Receptors	Compound ID	Docking score (kcal/mol)	Amino acids forming van der Waals interactions	Hydrogen	Amino acids forming other bonds
COX-2	268	-9.40	Ser353, Tyr355, Val116, Met113, Leu359, Ile345, Arg120, Leu531, Ser530, Gly526, Gly381, Trp387, Met522, Leu384, Phe518	Nil	Ala527, Leu352, Val523, Val349
	505	-9.30	Ser530, Tyr385, Phe381, Leu384, Gly526, Trp387, Met522, Phe518, Ser353, Tyr355, Met113, Val116	Nil	Ala527, val349, Leu531, Leu359, Val523, Leu352
	41	-9.00	Leu384, Trp387, Met522, Phe518, Leu352, Val523, Ser353, Tyr355, Val116, Leu359, Leu531, Val349, Ala527, Ser530, Tyr385, Phe381	Nil	Gly526
	1366	-8.80	Ser530, Phe381, Tyr385, Gly526, Trp387, Leu384, Met522, Leu352, Ser353	Nil	Leu531, Val349, Ala527, Tyr355, Val523
iNOS	981	-8.35	Trp346, Tyr347, Gln263, Ala351, Met374, Ile201	Gly371	Trp372, Val352, Glu377, Pro350, Tyr373, Arg388, Asp382
	41	-7.47	Trp463, Glu377, Cys200, Phe369, Val352, Pro350, Ala351, Gln263, Tyr347, Trp346, Asp382, Arg388, Glu377, Trp463	Nil	Tyr372
	2037	-7.15	Trp463, Tyr347, Trp346, Asp382, Arg388, Gln263, Val352, Gly371, Trp372, Ile201	Tyr373	Glu377, Pro350
	98	-7.13	Trp346, Asn370, TYR373, Glu377, Gly371, Phe369, Pro350, Ala351, Gln263, Arg388	Nil	Trp372, Val352, Asp382, Tyr347

Table 3: Pharmacokinetic properties of selected compounds along with reference drugs

S.No.	Parameters		Compound ID									Reference for COX-2	Reference for iNOS
			268	**505**	**1366**	**981**	**2037**	**98**	**2167**	**2058**	**41**	**Meclofenamic acid**	**AR-C95791**
1.	Absorption	GI Absorption	High	High	High	High	High	High	High	High	Yes	High	High
2.		P-GP Substrate	No	Yes	No	No	No	Yes	No	No	No	No	No
3.	Metabolism	CYP1A2 inhibitor	Yes	No	No	Yes	No	No	No	No	No	Yes	Yes
4.		CYP2C19 inhibitor	Yes	No	No	No	No	No	No	No	Yes	Yes	No
5.		CYP2C9 inhibitor	No	No	No	Yes	No	No	Yes	No	Yes	Yes	No
6.		CYP2D6 inhibitor	No	Yes	No	No	No	Yes	No	Yes	No	Yes	No
7.		CYP3A4 inhibitor	No	No	No	No	No	No	No	No	No	No	No
8.	Toxicity	Hepatotoxicity	-	-	-	-	-	-	-	-	-	Yes	-
9.		Carcinogenicity	-	-	-	-	-	-	-	-	-	-	-
10.		Mutagenicity	-	-	-	-	-	-	-	-	-	-	-
11.		Cytotoxicity	-	-	-	-	-	-	-	-	-	-	-
12.	Bioavailability Score		0.55	0.55	0.55	0.55	0.55	0.55	0.55	0.55	0.55	0.85	0.55
13.	PAINS alerts		0	0	0	0	0	0	0	0	0	0	0

Table 4: MM-PBSA free binding energy components (gas-phase, solvation, polar and non-polar contributions) calculated for the protein-ligand complexes during last 30 ns of MD simulation

S.No.	Target	Compound	**△E_vdW**	**△E_elec**	**△G_polar**	**△G_nonpolar**	**△G_bind**
1.	COX-2	Compound 41	-40.15	-19.77	42.48	-6.52	-24.95
		Meclofenamic acid (Reference drug)	-35.47	-69.52	84.31	-3.22	-23.90
2.	iNOS	Compound 41	-34.35	3.00	13.06	-3.12	-21.41
		AR-C95791 (Reference drug)	-27.67	-5.16	22.32	-3.17	-13.68

*△E_vdW = van der Waals Energy *△E_elec = Electrostatic energy *△G_polar = Polar Solvatoin Energy *△G_nonpolar = Non-polar Solvation Energy *△G_bind = Binding Free Energy

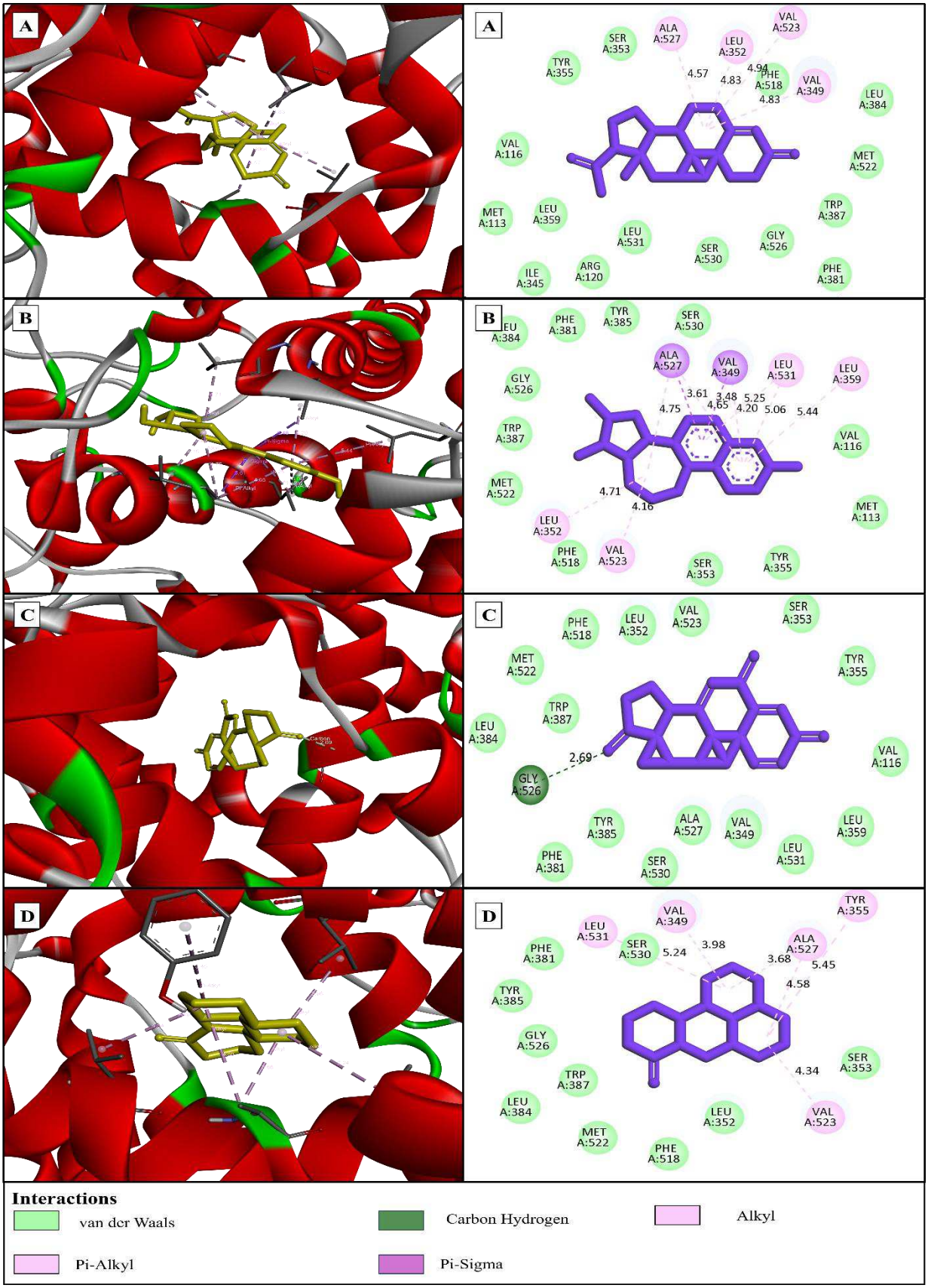


Figure 1: 3D (left) and 2D (right) binding interactions of COX-2 with ligands (A) Compound 268, (B) 505, (C) 41, and (D) 1366, showing key bonding interactions and bond distances.

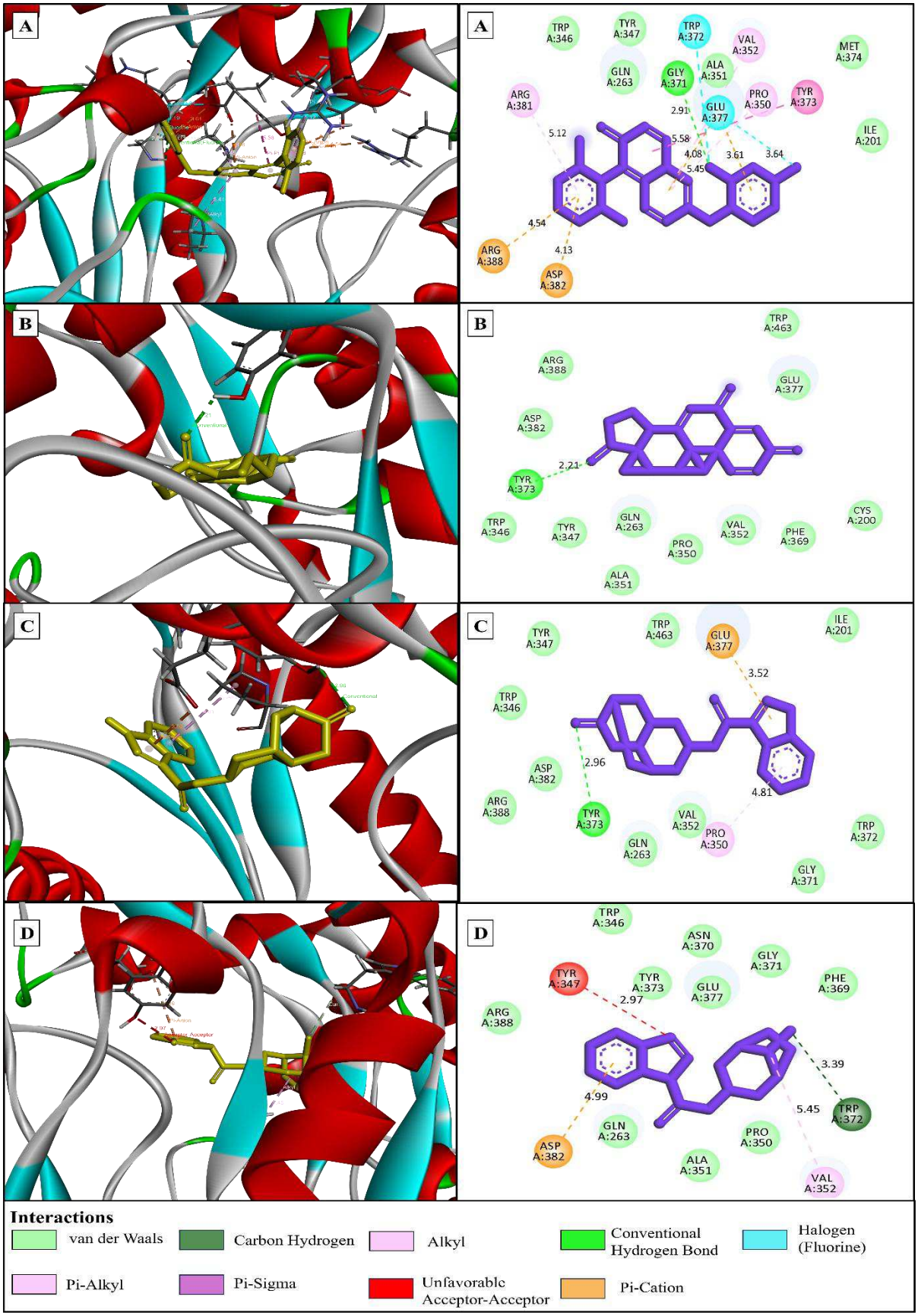


Figure 2: 3D (left) and 2D (right) binding interactions of iNOS with ligands (A) Compound 981, (B) 41, (C) 2037, and (D) 91, showing key bonding interactions and bond distances.

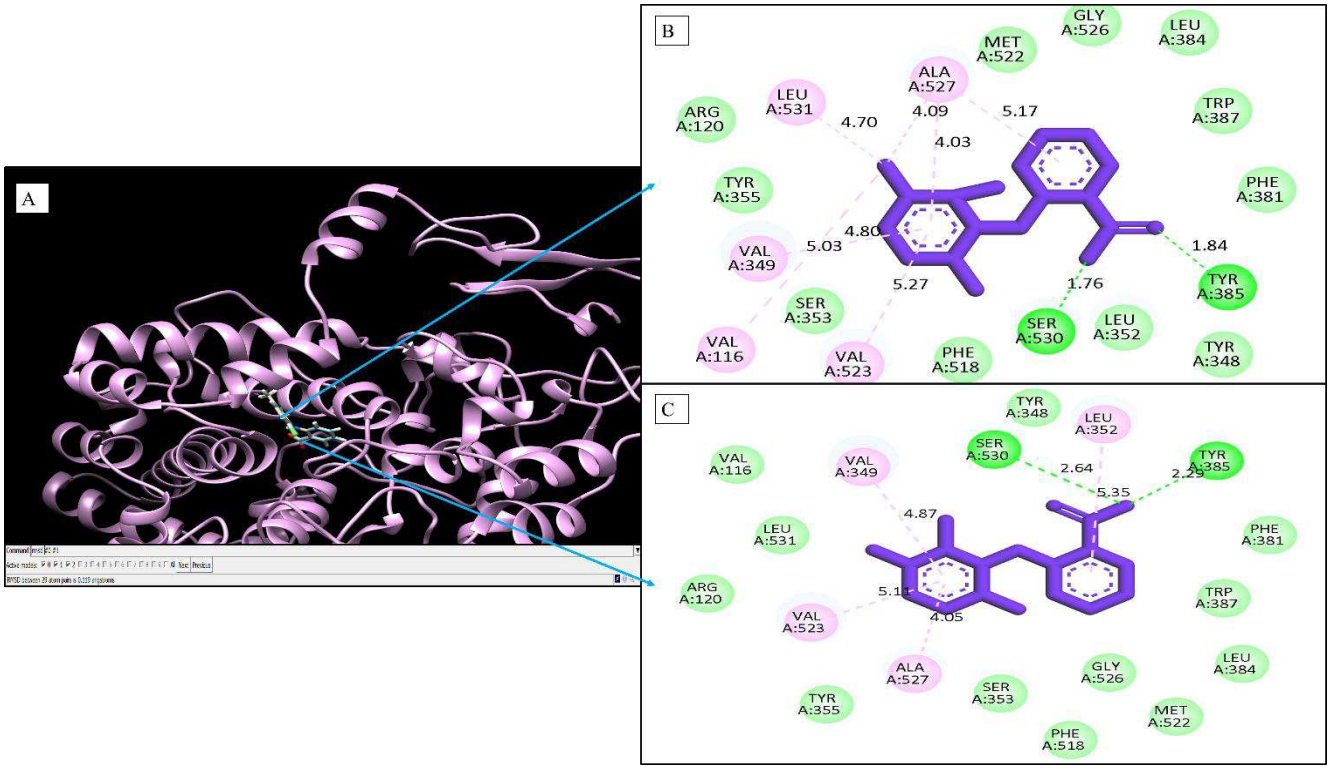


Figure 3: Redocking of the native ligand with COX-2 showing (A) superimposed poses and RMSD, (B) native ligand interactions, and (C) redocked ligand interactions highlighting conserved residues.

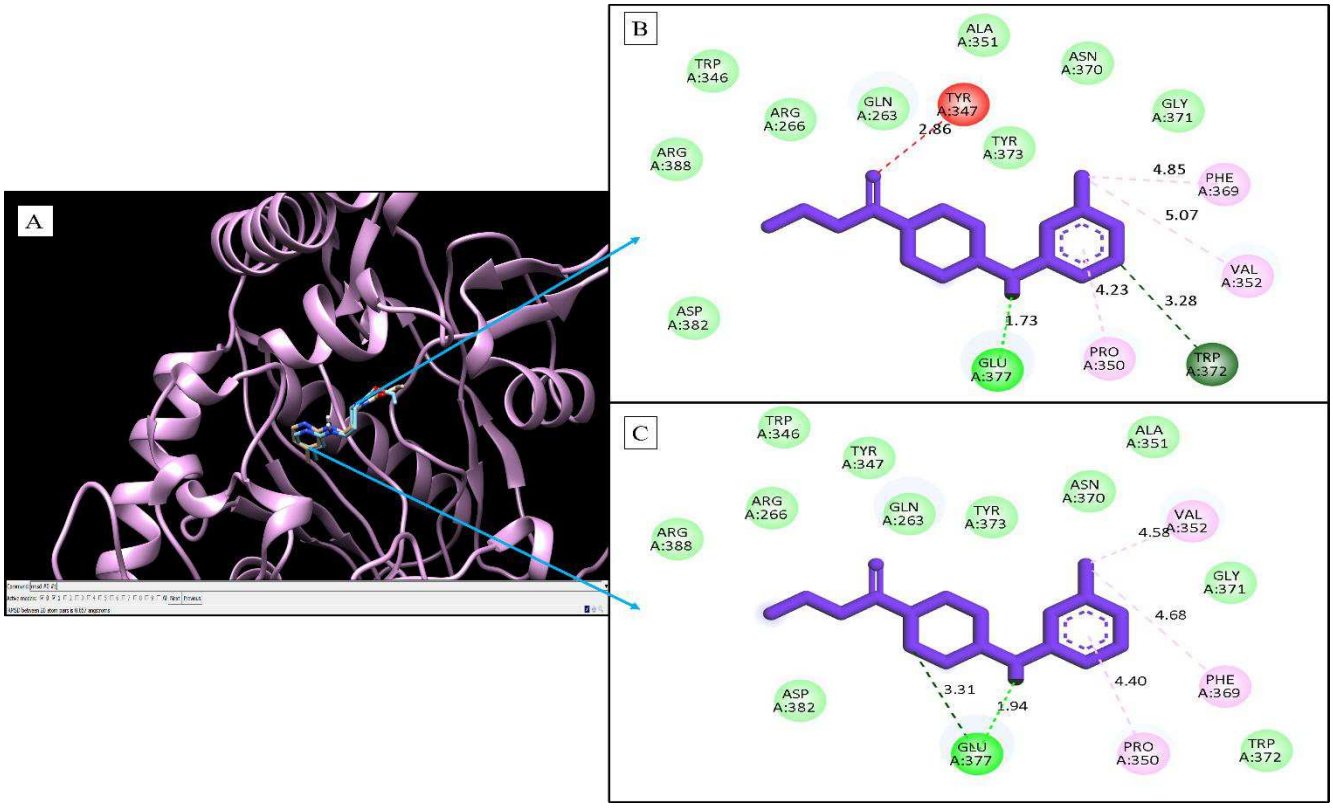


Figure 4: Redocking of the native ligand with iNOS showing (A) superimposed poses and RMSD, (B) native ligand interactions, and (C) redocked ligand interactions highlighting conserved residues.

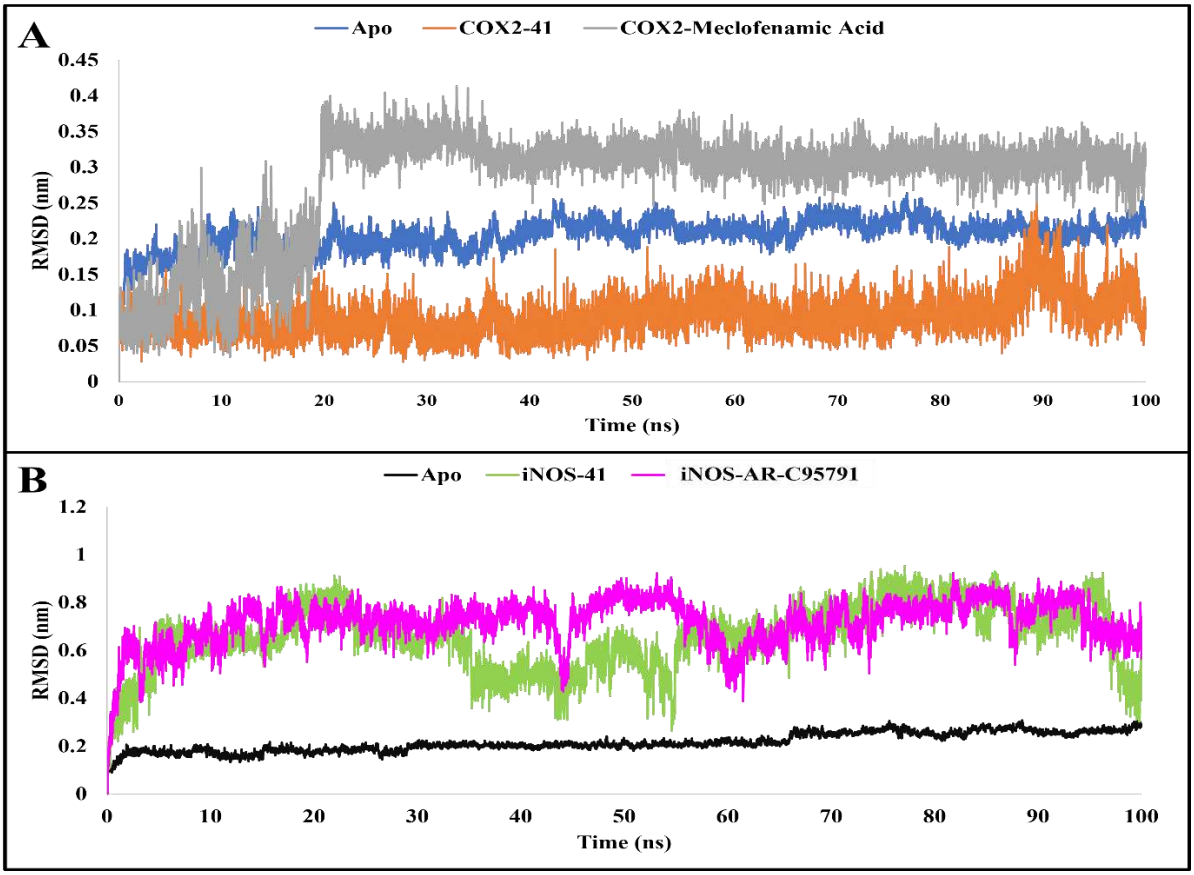


Figure 5: RMSD of different apo, protein-ligand and protein-reference drug bound systems (A) COX-2 (B) iNOS

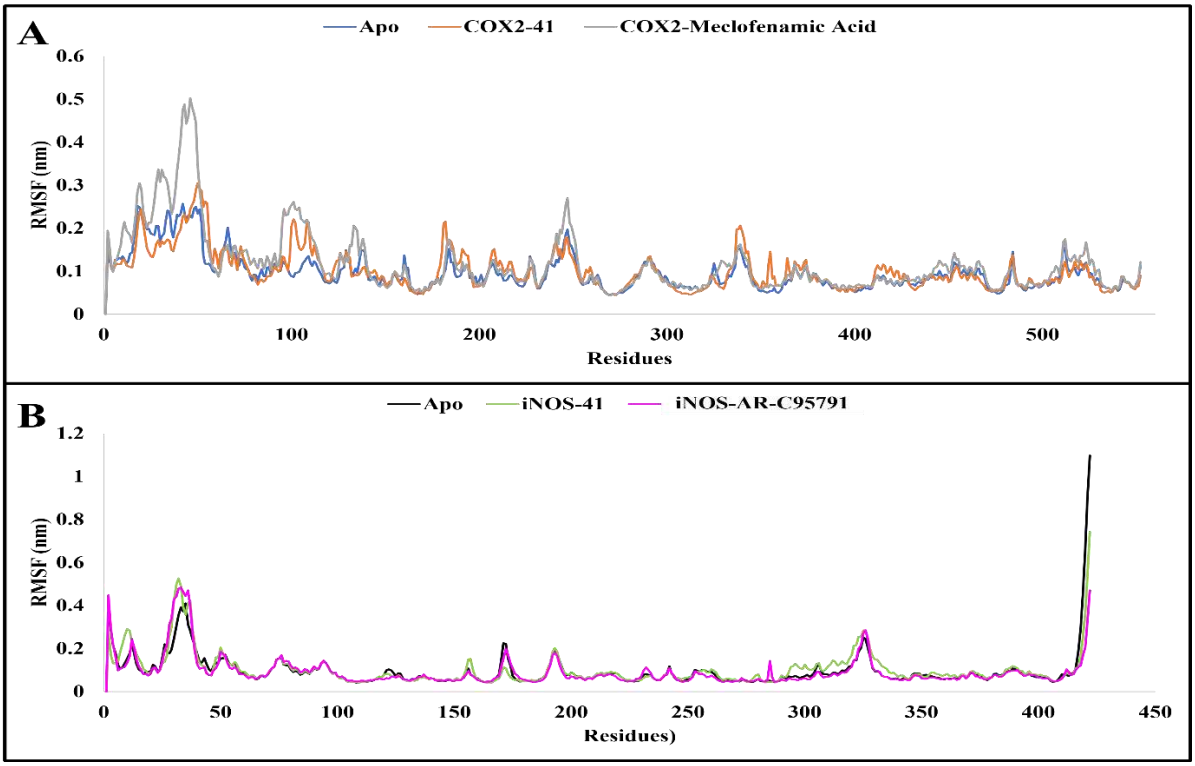


Figure 6: RMSF of different apo, protein-ligand and protein-reference drug bound systems (A) COX-2 (B) iNOS

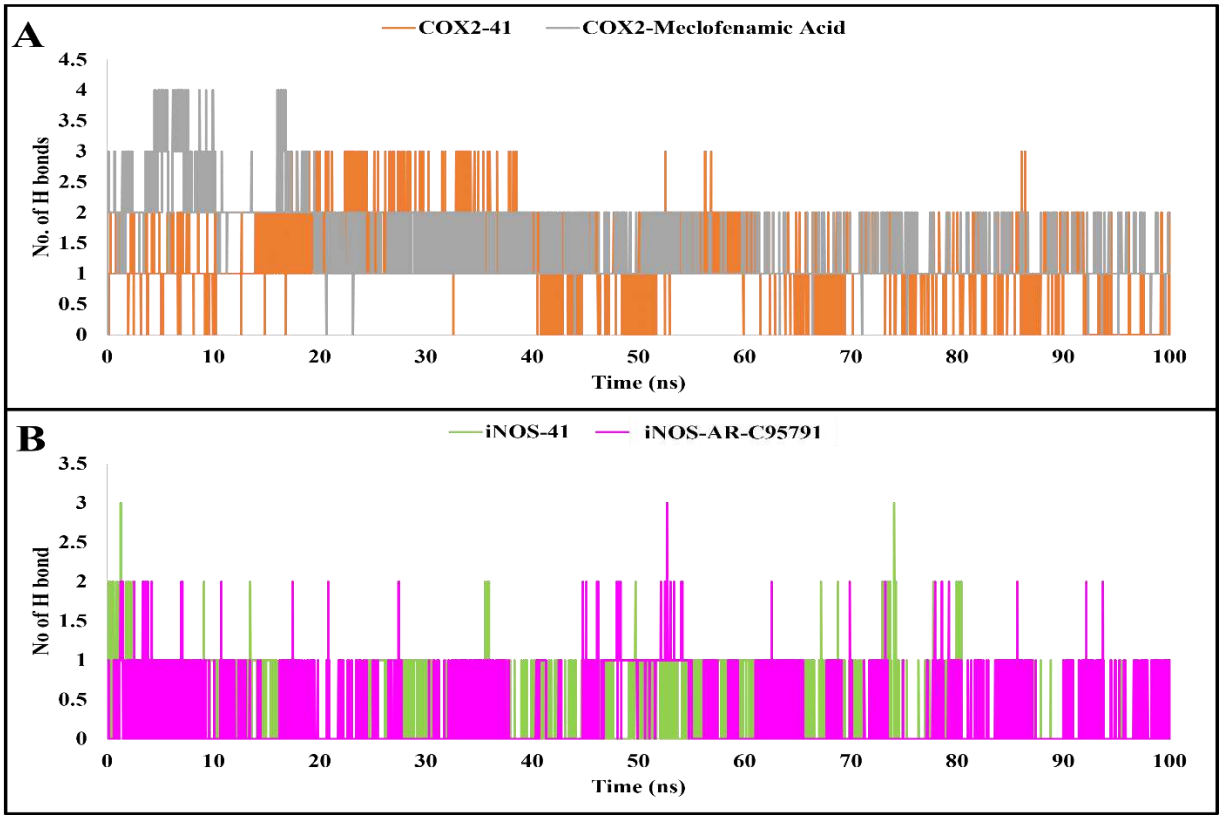


Figure 7: Hydrogen bond analysis of different protein-ligand and protein-reference drug bound systems (A) COX-2 (B) iNOS

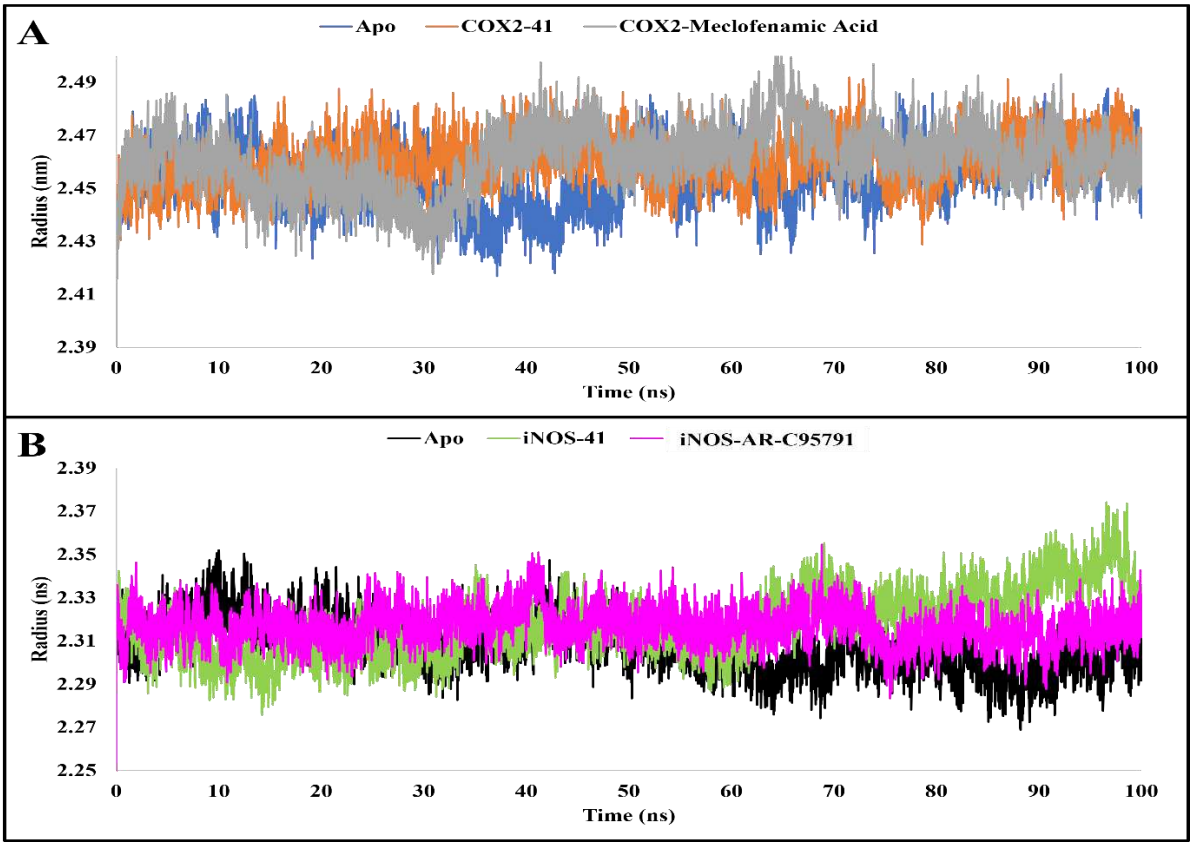


Figure 8: Rg of different apo, protein-ligand and protein-reference drug bound systems (A) COX-2 (B) iNOS

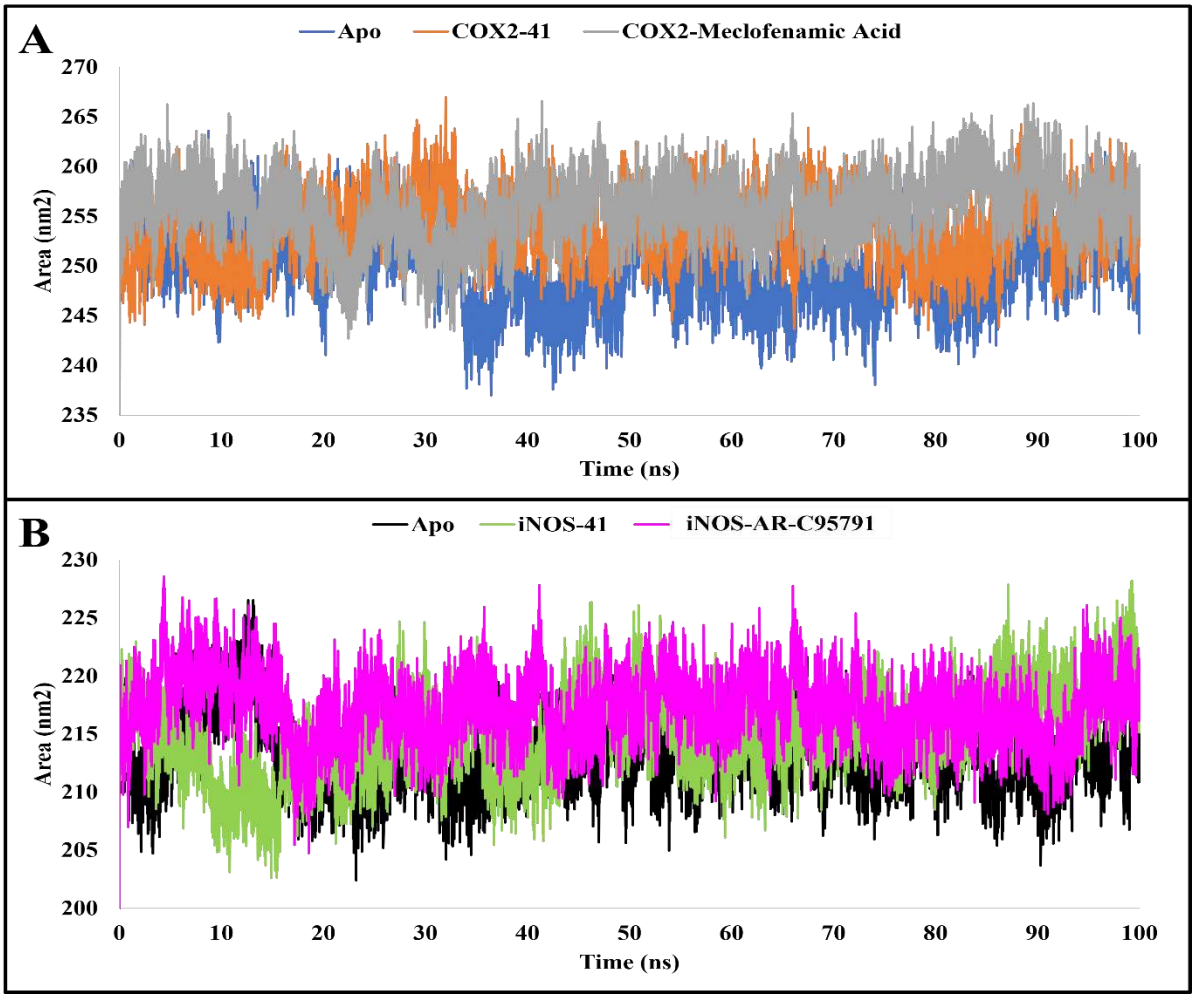


Figure 9: SASA of different apo, protein-ligand and protein-reference drug bound systems (A) COX-2 (B) iNOS

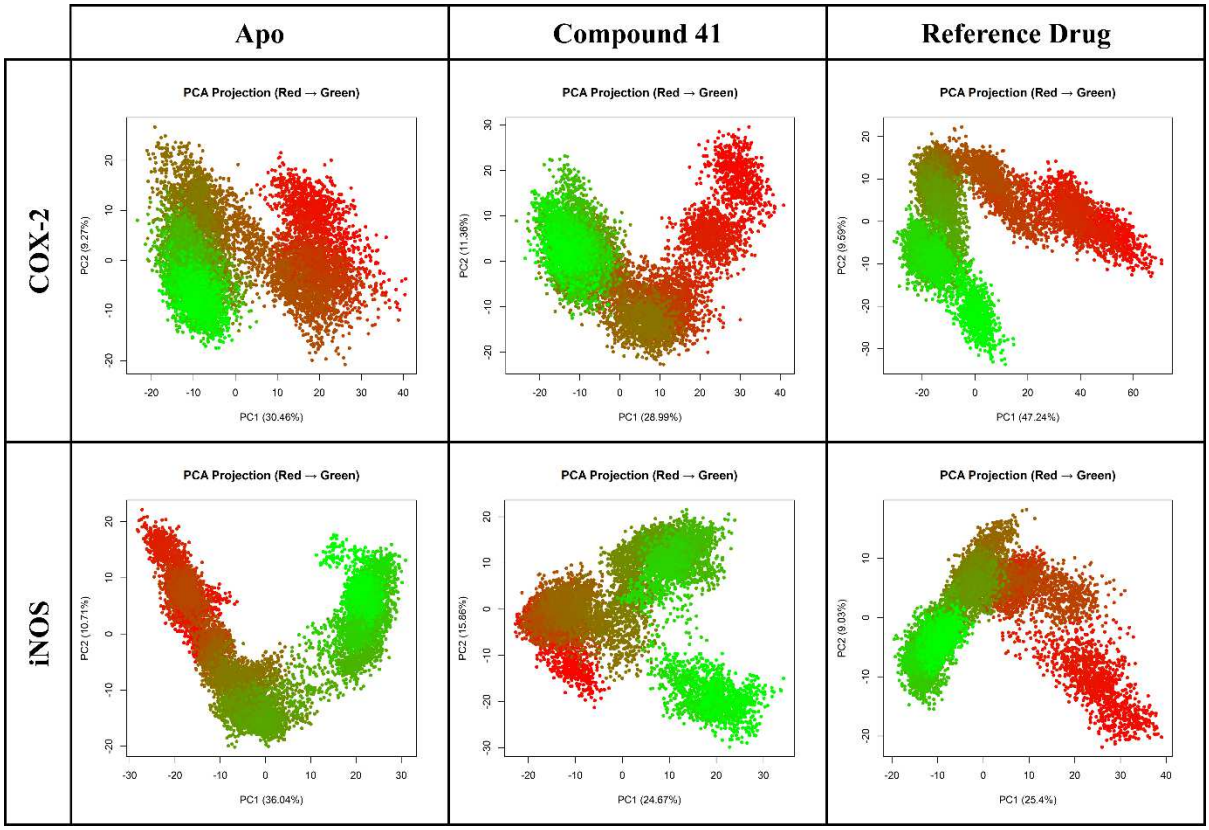


Figure 10: PCA of molecular dynamics trajectories for COX-2, and iNOS

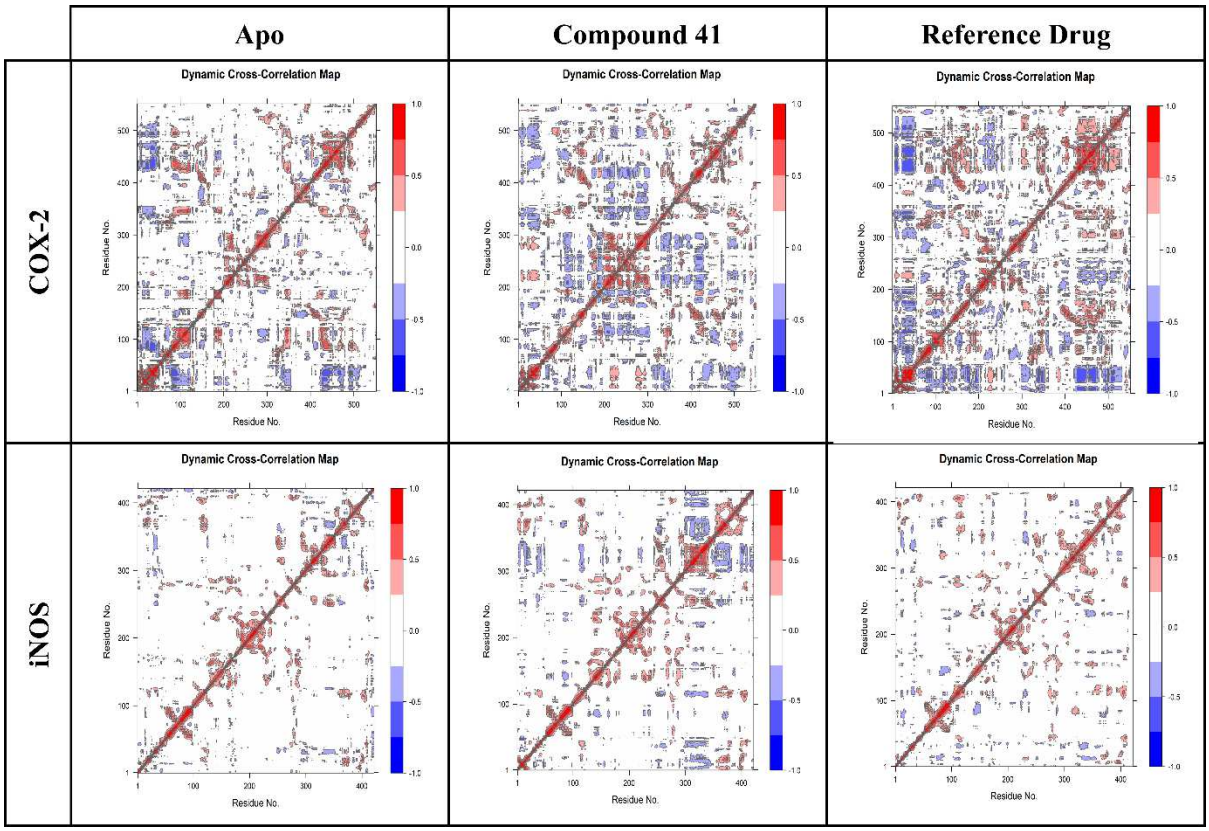


Figure 11: DCCM of molecular dynamics trajectories for COX-2, and iNOS

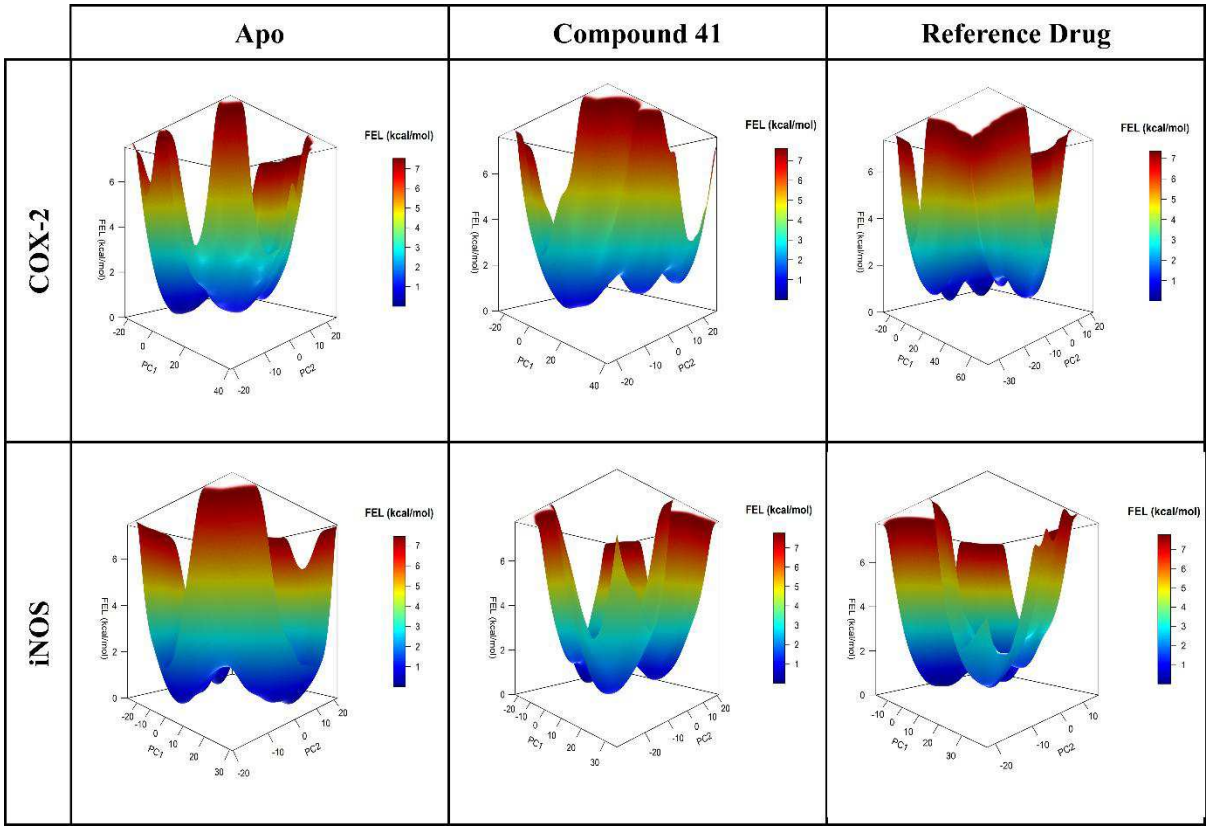


Figure 12: 3-Dimentional FEL of molecular dynamics trajectories for COX-2, and iNOS

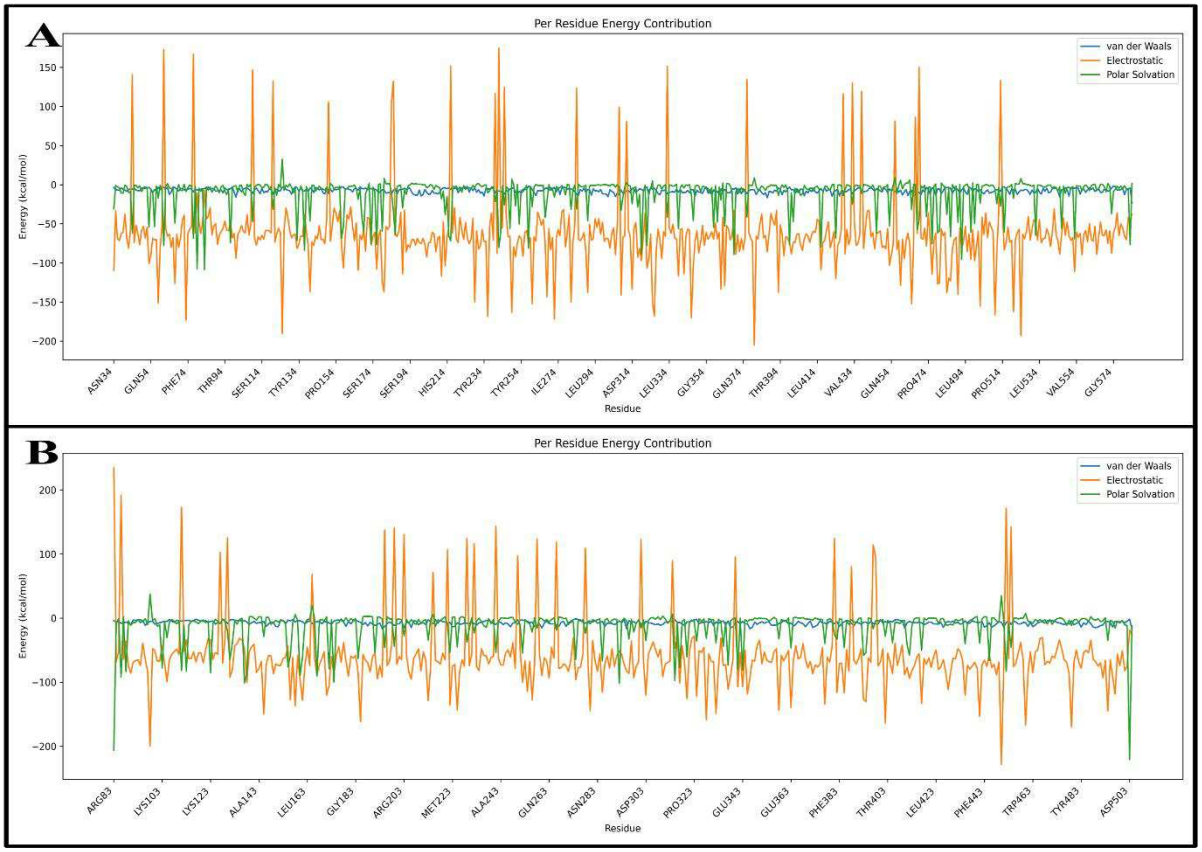


Figure 13: Per-residue free energy decomposition profiles for Compound 41 in complex with (A) COX-2, (B) iNOS.

References:

1. Alsedfy M Y, Ebnalwaled A A, Moustafa M, & Said A H (2024) Investigating the binding affinity, molecular dynamics, and ADMET properties of curcumin–IONPs as a mucoadhesive bioavailable oral treatment for iron deficiency anemia. Scientific Reports. https://doi.org/10.1038/s41598-024-72577-8
2. Banerjee P, Kemmler E, Dunkel M, & Preissner R (2024) ProTox 3.0: a webserver for the prediction of toxicity of chemicals. Nucleic acids research. https://doi.org/10.1093/nar/gkae303
3. Baral D S, & Verma R (2025) Discovery and identification of bioactive organic compounds from Callistemon citrinus (bottlebrush) as natural inhibitors of acetylcholinesterase via the cholinergic pathway for Alzheimer's disease management. ChemistrySelect. https://doi.org/10.1002/slct.202504550
4. Baral D S, & Verma R (2025) Discovery of natural PDE-5 inhibitors in NO signalling pathways for human erectile dysfunction management: A multi-layered in silico assessment. In Silico Pharmacology. https://doi.org/10.1007/s40203-025-00491-6
5. Bell S G, Dalton L, McNeish B L, Fang F, Henry N L, Kidwell K M, & McLean K (2020) Aromatase inhibitor use, side effects and discontinuation rates in gynecologic oncology patients. Gynecologic oncology. https://doi.org/10.1016/j.ygyno.2020.08.015
6. Bussi G, Donadio D, & Parrinello M (2007) Canonical sampling through velocity rescaling. The Journal of Chemical Physics. https://doi.org/10.1063/1.2408420
7. Chachlaki K, & Prevot V (2020) Nitric oxide signalling in the brain and its control of bodily functions. British Journal of Pharmacology. https://doi.org/10.1111/bph.14800
8. Christoffel D J, Golden S A, & Russo S J (2011) Structural and synaptic plasticity in stress-related disorders. Reviews in the Neurosciences. https://doi.org/10.1515/RNS.2011.044
9. Daina A, Michielin O, & Zoete V (2017) SwissADME: A free web tool to evaluate pharmacokinetics, drug-likeness and medicinal chemistry friendliness of small molecules. Scientific Reports. https://doi.org/10.1038/srep42717
10. Dash R, Arifuzzaman M, Mitra S, Abdul Hannan M, Absar N, & Hosen S Z (2019) Unveiling the structural insights into the selective inhibition of protein kinase D1. Current Pharmaceutical Design. https://doi.org/10.2174/1381612825666190527095510
11. de Oliveira T A, Medaglia L R, Maia E H B, Assis L C, de Carvalho P B, da Silva A M, & Taranto A G (2022) Evaluation of docking machine learning and molecular dynamics methodologies for DNA-ligand systems. Pharmaceuticals. https://doi.org/10.3390/ph15020132
12. Eberhardt J, Santos-Martins D, Tillack A F, & Forli S (2021) AutoDock Vina 1.2. 0: new docking methods, expanded force field, and python bindings. Journal of chemical information and modeling. https://doi.org/10.1021/acs.jcim.1c00203
13. Genheden S, & Ryde U (2015) The MM/PBSA and MM/GBSA methods to estimate ligand-binding affinities. Expert Opinion on Drug Discovery. https://doi.org/10.1517/17460441.2015.1032936
14. Ghahremanian S, Rashidi M M, Raeisi K, & Toghraie D (2022) Molecular dynamics simulation approach for discovering potential inhibitors against SARS-CoV-2: A structural review. Journal of molecular liquids. https://doi.org/10.1016/j.molliq.2022.118901
15. Hassan A M, Gattan H S, Faizo A A, Alruhaili M H, Alharbi A S, Bajrai L H, & Azhar E I (2024) Evaluating the binding potential and stability of drug-like compounds with the monkeypox virus VP39

protein using molecular dynamics simulations and free energy analysis. Pharmaceuticals. https://doi.org/10.3390/ph17121617

16. Huang J, & MacKerell A D, Jr (2013) CHARMM36 all-atom additive protein force field: Validation based on comparison to NMR data. Journal of Computational Chemistry. https://doi.org/10.1002/jcc.23354
17. Iova O M, Marin G E, Lazar I, Stanescu I, Dogaru G, Nicula C A, & Bulboaca A E (2023) Nitric oxide/nitric oxide synthase system in the pathogenesis of neurodegenerative disorders—An overview. Antioxidants. https://doi.org/10.3390/antiox12030753
18. Islam M T, Aktaruzzaman M, Barai C, Rafi F I, Hasan A R, Tasnim T, & Raihan M O (2025) In silico screening of naturally derived dietary compounds as potential butyrylcholinesterase inhibitors for Alzheimer's disease treatment. Scientific Reports. https://doi.org/10.1038/s41598-025-98092-y
19. Kaufmann W E, Worley P F, Pegg J, Bremer M, & Isakson P (1996) COX-2, a synaptically induced enzyme, is expressed by excitatory neurons at postsynaptic sites in rat cerebral cortex. Proceedings of the National Academy of Sciences of the United States of America. https://doi.org/10.1073/pnas.93.6.2317
20. Khalid M, Alqarni M H, Shoaib A, Wahab S, Foudah A I, Aljarba T M, & Ahmad S (2022) Anti-obesity action of Boerhavia diffusa in rats against high-fat diet-induced obesity by blocking the cannabinoid receptors. Plants. https://doi.org/10.3390/plants11091158
21. Kittaneh M, & Gluck S (2011) Aromasin in the adjuvant treatment of breast cancer in postmenopausal women. Breast Cancer: Basic and Clinical Research. https://doi.org/10.4137/BCBCR.S6234
22. Kulkarni V S, Alagarsamy V, Solomon V R, Jose P A, & Murugesan S (2023) Drug repurposing: an effective tool in modern drug discovery. Russian journal of bioorganic chemistry. https://doi.org/10.1134/S1068162023020139
23. Li R, Singh R, Kashav T, Yang C, Sharma R D, Lynn A M, & Kumar V (2022) Computational Insights of unfolding of N-terminal domain of TDP-43 reveal the conformational heterogeneity in the unfolding pathway. Frontiers in Molecular Neuroscience. https://doi.org/10.3389/fnmol.2022.822863
24. Lisman J (2017) Glutamatergic synapses are structurally and biochemically complex due to multiple plasticity processes. Philosophical Transactions of the Royal Society B: Biological Sciences. https://doi.org/10.1098/rstb.2016.0260
25. Liu H, & Talalay P (2013) Relevance of anti-inflammatory and antioxidant activities of Aromasin and synergism with sulforaphane for disease prevention. Proceedings of the National Academy of Sciences of the United States of America. https://doi.org/10.1073/pnas.1318247110
26. Moussa N, & Dayoub N (2023) Exploring the role of COX-2 in Alzheimer's disease: Potential therapeutic implications of COX-2 inhibitors. Saudi Pharmaceutical Journal. https://doi.org/10.1016/j.jsps.2023.101729
27. O'Boyle N M, Banck M, James C A, Morley C, Vandermeersch T, & Hutchison G R (2011) Open Babel: An open chemical toolbox. Journal of cheminformatics. https://doi.org/10.1186/1758-2946-3-33
28. Odhiambo D O, Omosa L K, Njagi E C, Kithure J G, & Wekesa E N (2025) In-silico pharmacokinetics ADME/Tox analysis of phytochemicals from genus Dracaena for their therapeutic potential. Scientific African. https://doi.org/10.1016/j.sciaf.2025.e02796

29. Pacher P, Beckman J S, & Liaudet L (2007) Nitric oxide and peroxynitrite in health and disease. Physiological Reviews. https://doi.org/10.1152/physrev.00029.2006
30. Pajouhesh H, & Lenz G R (2005) Medicinal chemical properties of successful central nervous system drugs. NeuroRx. https://doi.org/10.1602/neurorx.2.4.541
31. Pakrashy S, Mandal P K, Dey S K, Choudhury S M, Alasmary F A, Almalki A S, & Dolai M (2022) Design of a structurally novel multipotent drug candidate by the Scaffold architecture technique for ACE-II, NSP15, and Mpro protein inhibition: Identification and isolation of a natural product to prevent the severity of future variants of Covid 19 and a colorectal anticancer drug. ACS omega. https://doi.org/10.1021/acsomega.2c04051
32. Pandey B, Grover A, & Sharma P (2018) Molecular dynamics simulations reveal structural differences among WRKY domain–DNA interactions in barley. BMC Genomics. https://doi.org/10.1186/s12864-018-4506-3
33. Parrinello M, & Rahman A (1981) Polymorphic transitions in single crystals: A new molecular dynamics method. Journal of Applied Physics. https://doi.org/10.1063/1.328693
34. Rana N, Solanki P, Mehra R, & Manhas A (2025) Identification of natural compound inhibitors for substrate-binding site of MTHFD2 enzyme: Insights from structure-based drug design and biomolecular simulations. Chemical Physics Impact. https://doi.org/10.1016/j.chphi.2024.100809
35. Samanta S, Ramesh M, & Govindaraju T (2022) Recent findings in pathophysiology, diagnostic and therapeutic modalities. In: T. Govindaraju (Ed.), Alzheimer's disease, Royal Society of Chemistry, (pp. 1–34) https://doi.org/10.1039/9781839162732-00001
36. Shankar G M, & Walsh D M (2009) Alzheimer's disease: Synaptic dysfunction and Aβ. Molecular Neurodegeneration. https://doi.org/10.1186/1750-1326-4-48
37. Simpkins J W, Singh M, Brock C, & Etgen A M (2012) Neuroprotection and estrogen receptors. Neuroendocrinology. https://doi.org/10.1159/000338409
38. Skjaerven L, Yao X Q, Scarabelli G, & Grant B J (2014) Integrating protein structural dynamics and evolutionary analysis with Bio3D. BMC Bioinformatics. https://doi.org/10.1186/s12859-014-0399-6
39. Stefanovic B, Bosetti F, & Silva A C (2006) Modulatory role of cyclooxygenase-2 in cerebrovascular coupling. NeuroImage. https://doi.org/10.1016/j.neuroimage.2006.03.014
40. Tewari D, Sah A N, Bawari S, Nabavi S F, Dehpour A R, Shirooie S, & Nabavi S M (2021) Role of nitric oxide in neurodegeneration: function, regulation, and inhibition. Current neuropharmacology. https://doi.org/10.2174/1570159X18666200429001549
41. Torres D M C, & Cardenas F P (2020) Synaptic plasticity in Alzheimer's disease and healthy aging. Reviews in the Neurosciences. https://doi.org/10.1515/revneuro-2019-0058
42. Valdes-Tresanco M S, Valdes-Tresanco M E, Valiente P A, & Moreno E (2021) gmx_MMPBSA: a new tool to perform end-state free energy calculations with GROMACS. Journal of chemical theory and computation. https://doi.org/10.1021/acs.jctc.1c00645
43. Wang S, Sun X, Cui W, & Yuan S (2022) MM/PB (GB) SA benchmarks on soluble proteins and membrane proteins. Frontiers in Pharmacology. https://doi.org/10.3389/fphar.2022.1018351

44. Woodling N S, Colas D, Wang Q, Minhas P, Panchal M, Liang X, & Andreasson K I (2016) Cyclooxygenase inhibition targets neurons to prevent early behavioural decline in Alzheimer's disease model mice. Brain. https://doi.org/10.1093/brain/aww117
45. World Health Organization. (2024). World health statistics 2024: Monitoring health for the SDGs. World Health Organization.
46. Yang H, & Chen C (2008) Cyclooxygenase-2 in synaptic signaling. Current Pharmaceutical Design, 14:1443–1451.
47. Zhang W, Xiao D, Mao Q, & Xia H (2023) Role of neuroinflammation in neurodegeneration development. Signal Transduction and Targeted Therapy. https://doi.org/10.1038/s41392-023-01486-5
48. Zhang X, Chen Z, Xiong Y, Zhou Q, Zhu L, & Liu D (2024) Emerging role of nitric oxide in synaptic dysfunction of vascular dementia. Neural Regeneration Research 20:402–415.

Supplementary Files

This is a list of supplementary files associated with this preprint. Click to download.

- Supplementary.xlsx